DR LIANG XUE (Orcid ID : 0000-0003-4206-2800)

Article type : Research Article

Use of neomycin as a structured amino-containing side chain motif for phenanthroline based G-quadruplex ligands and telomerase inhibitors

Mandeep Singh,[1] Siwen Wang,[1] Hyun Joo,[1] Zhihan Ye,[1] Krege M. Christison,[1] Ryan Hekman,[2] Craig Vierra,[2] and Liang Xue[1]*

[1]Department of Chemistry, University of the Pacific, 3601 Pacific Avenue, Stockton, California 95211 (USA)

[2]Department of Biological Sciences, University of the Pacific, Stockton, California 95211 (USA)

*Corresponding author:

Tel: 1-209-946-2360; Fax: 1-209-946-2607; Email: lxue@pacific.edu

Keywords: G-quadruplex DNA, DNA binding ligands, phenanthroline, neomycin, telomerase inhibition

Abbreviations

G4 ligands, G-quadruplex ligands; BIBR, 2-[[(2*E*)-3-(2-naphthalenyl)-1-oxo-2-butenyl-1-yl]amino]benzoic acid; TMPyP4, meso-tetra(N-methyl-4-pyridyl)porphyrin tetratosylate; BRACO-19, N,N′-(9-(4-(Dimethylamino)phenylamino)acridine-3,6-diyl)bis(3-(pyrrolidin-1-yl)propanamide); DMF, dimethylformamide; TCDP, 1,1'-thiocarbonyldi-1(1H)-pyridone; TO, thiazole orange; TLC, thin-layer chromatography; CD, circular dichroism; ITC, isothermal titration calorimetry; TRAP, telomeric repeat amplification protocol; FID, fluorescent intercalator displacement

Abstract

In this paper, we report the synthesis of a phenanthroline and neomycin conjugate (**7**). Compound **7** binds to a human telomeric G-quadruplex (**G1**) with a higher affinity compared with its parent compounds (phenanthroline and neomycin), which is determined by several biophysical studies. Compound **7** shows good selectivity for G-quadruplex (G4) DNA over duplex DNA. The binding of **7** with **G1** is predominantly enthalpy-driven, and the binding stoichiometry of **7** with **G1** is one for the tight-binding event as determined by ESI mass spectrometry. A plausible binding mode is a synergistic effect of end-stacking and groove interactions, as indicated by docking studies. Compound **7** can inhibit human telomerase activity at low micromolar concentrations, which is more potent than previously reported 5-substituted phenanthroline derivatives.

1. Introduction

G-quadruplex (G4) DNA is a unique DNA secondary structure formed via self-assembly of guanines in a G-rich sequence under physiological conditions (1, 2). The formation of G4s occurs *in vivo* (3). Initial surveys suggested that over 300,000 putative G-quadruplex forming sequences are present in the human genome (4, 5), and recent studies predicted an even higher G4 prevalence when considering G4s with long loops (6) and G4s in some large genes (7), implying that a structure-function relationship may exist. In recent years, G4s have emerged as a target of considerable interest because they are not native substrates for binding of nucleic acid processing enzymes (e.g., telomerase and polymerase); therefore, inducing G4 formation has been recognized as a promising approach to regulate enzymatic functions (8-10), for instance, inhibition of human telomerase activity (11-13) and regulation of oncogene expression (14, 15). In addition, G4s could activate DNA damage responses (16).

Small molecules known as G4 ligands facilitate the formation and stabilization of G4s (17, 18). Most of the G4 ligands developed so far contain a large aromatic surface that effectively stacks with G-quartet(s) at the ends of G4s (end-stacking mode) (19-21). Phenanthroline derivatives are examples of G4 ligands that have been extensively studied (11, 22-27). 1,10-Phenanthroline (Phen) alone does not bind to G4s. When Phen coordinates with metal ions such as $Ni^{2+}$and Pt^{2+}, the resulting complex becomes a potent G4 ligand due to the enlarged aromatic stacking surface. In a recent study of 5-substituted phenanthrolines, we reported that aromatic side chains (arylsulfanyl group) at the 5-position of Phen provide the best selectivity for G4 over duplex DNA (11). On the other hand, amino-containing side chains (piperidine, pyrrolidine) showed enhanced binding affinity but decreased binding selectivity for G4 over duplex DNA. Similar results have also been reported in our study of thiazole orange derivatives as G4 ligands (12) and by others (28, 29). The decreased selectivity could result from non-specific interactions between positively charged amino groups and DNA backbones. We believe that it is possible to create more selective and potent phenanthroline-based G4 ligands using structured side chains containing positive charges such as neomycin. Neomycin contains six amino groups that are protonated or partially protonated under physiological conditions (30). More importantly, these amino groups are spatially arranged via saccharide linkage to create a structured binding motif. Masking all six amino groups of neomycin with a *tert*-butoxycarbonyl (Boc) group

drastically reduces its binding ability to nucleic acids (unpublished data in the group). Neomycin is known to bind to the A site of 16S rRNA (31) and various A-form-like nucleic acid structures (32). It has also been reported that neomycin binds to an *Oxytricha nova* G-quadruplex via groove binding, but the binding affinity is rather moderate (33). A series of neomycin-capped macrocyclic molecules have been studied for G-quadruplex DNA recognition (34). Arya's group has done pioneering work by developing a series of neomycin conjugates that show a significant synergistic effect on binding to various DNA structures, including triplex DNA (35-37) and G-quadruplex DNA (38, 39). As a continuation of our study on Phen-based G4 ligands, we herein report the synthesis of a phenanthroline-neomycin conjugate and evaluation of its binding to a telomeric G-quadruplex and inhibition of human telomerase activity.

2. Experimental section

2.1. Materials and General Methods

All the chemicals for synthesis were purchased from Sigma-Aldrich or Fisher Scientific and used without further purification. DNA oligonucleotides were synthesized on an ABI 392 DNA/RNA synthesizer using standard phosphoramidite protocols and purified using polyacrylamide gel electrophoresis. All reagents and solid-support columns for DNA synthesis were purchased from Glen Research. The concentrations of DNA solutions were determined by UV spectroscopy, using the molar extinction coefficients (in units of mol of strand/L^{-1} cm^{-1}) obtained from OligoAnalyzer (www.idtdna.com). ε_{260} = 237,000 for **G1** [5'-AGGG(TTAGGG)$_3$T-3']; ε_{260} = 259,100 for **S1** (5'-ATGAAGGACGTAACCGGCTCTGAACG-3'); ε_{260} = 167,400 for **S2** (5'-CGTTCAGAGCCGGTTACGTCCTTCAT-3'); ε_{260} = 238,300 for TS primer (5'-AATCCGTCGAGCAGAGTT-3'); ε_{260} = 261,000 for RP (5'-GCGCGGCTTACCCTTACCCTTACCCTAACC-3'); ε_{260} = 151,800 for NT (5'-ATCGCTTCTCGGCCTTTT-3'); ε_{260} = 370,100 for TSNT (5'-AATCCGTCGAGCAGAGTTAAAAGGCCGAGAAGCGAT-3'). ^{1}H NMR and ^{13}C NMR spectra were collected on a JEOL ECA 600 MHz FT-NMR spectrometer. Mass spectra of the synthesized compounds were analyzed on an Agilent 1290 UHPLC coupled to an Agilent 6230 Time-of-Flight mass spectrometer. Mass spectra of ligand-DNA complexes were collected on a Thermo Fisher Orbitrap Fusion Tribrid Mass Spectrometer. UV spectra were recorded on a Varian Cary 100 Bio UV-

Vis spectrophotometer equipped with a thermoelectrically controlled 6 × 6 cell holder. Circular dichroism spectra were recorded on a JASCO J-810 spectropolarimeter using a quartz cuvette with a 1 mm or 1 cm optical path length. Isothermal microcalorimetric measurements were performed on a TA Instruments Affinity ITC LV. T4 polynucleotide kinase was obtained from New England Biolabs. [γ-^{32}P]-ATP was purchased from MP Biochemicals. Quantification of 5' ^{32}P-labeled oligonucleotides was carried out using a Storm 860 phosphorimager and ImageQuant 5.1 software. Cell medium and supplements (fetal bovine serum, L-glutamine, antimycotic) were acquired from Invitrogen. HeLa cells were maintained in advanced DMEM/F12 medium supplemented with 5% fetal bovine serum, L-glutamine, and antimycotic at 37 °C in a humid atmosphere containing 5% CO_2. DNA labeling was performed by incubating [γ-^{32}P]-ATP (30 μCi) and T4 polynucleotide kinase (20 units) in the presence of an oligonucleotide (10 pmol) at 37°C for 30 min. Unreacted [γ-^{32}P]-ATP was removed using a MicroSpin G-25 column.

*2.2. Synthesis of **6***

In 25 mL round-bottomed flask, **5** (46.8 mg, 0.0385 mmol) was dissolved in anhydrous pyridine (5 mL). An anhydrous pyridine solution (1 mL) of compound **9** (10.4 mg, 0.0350 mmol) was added dropwise into the flask with a syringe. The reaction mixture was stirred overnight at room temperature under N_2 and concentrated under vacuum. Flash chromatography of the residue [silica gel, CH_3OH:CH_2Cl_2:NH_4OH = 8:92:0.8 (v/v/v)] yielded compound **6** (R_f = 0.30; 23.7 mg, 40.7 %). IR (KBr, cm^{-1}) 3340, 2976, 2920, 2851, 1685, 1521, 1384, 1252, 1174, 1031. ^{1}H NMR (600 MHz, CD_3OD): ^{1}H NMR (600 MHz, CD_3OD): δ 9.11 (dd, *J* = 4.2, 1.8 Hz, 1H), 9.00 (dd, *J* = 4.2, 1.8 Hz, 1H), 8.83 (dd, *J* = 8.4, 1.8 Hz, 1H), 8.41 (dd, *J* = 7.8, 1.8 Hz, 1H), 8.35 (s, 1H), 7.82 (q, *J* = 4.2 Hz, 1H), 7.76 (q, *J* = 4.2 Hz, 1H), 6.59 - 6.94 (m, 2H), 5.51 (s, 1H), 5.03 (s, 1H), 4.24 - 4.55 (m, 2H), 3.68 - 4.21 (m, 8H), 3.69 - 3.79 (m, 2H), 3.45 - 3.64 (m, 6H), 3.06 - 3.22 (m, 3H), 1.88 - 1.99 (m, 1H), 1.27 - 1.57 (m, 54H). HRMS (ESI) calcd for $C_{68}H_{107}N_{10}O_{24}S_2$ $[M+H]^+$: 1511.6901, found 1511.6894.

*2.3. Synthesis of **7***

Compound **6** (6.00 mg, 0.00397 mmol) was dissolved in trifluoroacetic acid (2 mL) and stirred for 15 min. The reaction mixture was concentrated on a rotavapor under vacuum. The residue was dissolved in water (1 mL), and the aqueous solution was washed with dichloromethane (3 × 3 mL). Lyophilization yielded compound **7** (5.00 mg, 78.9%). IR (KBr, cm^{-1}) 3431, 2920, 2850, 1624, 1500,

1384, 1040. ^{1}H NMR (600 MHz, D_2O): δ 9.09 (d, *J* = 4.3 Hz, 1H), 8.89 - 9.03 (m, 2H), 8.76 (d, *J* = 8.4 Hz, 1H), 8.18 (s, 1H), 8.02 (dd, *J* = 8.4, 5.4 Hz, 1H), 7.97 (dd, *J* = 8.4, 4.8 Hz, 1H), 5.90 (d, *J* = 3 Hz, 1H), 5.27 (d, *J* = 3 Hz, 1H), 5.12 (s, 1H), 4.65 (s, 2H), 4.31 (t, *J* = 4.8 Hz, 1H), 4.02 - 4.26 (m, 3H), 3.97 (t, *J* = 10.2 Hz, 1H), 3.50 - 3.92 (m, 8H), 3.05 – 3.50 (m, 11H), 2.35 (dt, *J* = 8.4, 2.4 Hz, 1H), 1.75 (q, *J* = 13.2 Hz, 1H). HRMS (ESI) calcd for $C_{38}H_{60}N_{10}O_{12}S_2$ $[M+H]^+$: 911.3755, found 911.3754.

2.4. Synthesis of ***9***

In a 25 mL round-bottomed flask, compound **8** (80.0 mg, 0.314 mmol) and DMAP (catalytic amount) were dissolved in DMF (10 mL) under N_2. A DMF solution (1 mL) of TCDP (109 mg, 0.471 mmol) was added dropwise into the flask using a syringe and the resulting mixture was stirred overnight at room temperature. The completion of the reaction was monitored by TLC [R_f = 0.52, CH_3OH:CH_2Cl_2:NH_4OH=8:92:0.5 (v/v), silica gel 60 F_{254}, EMD Millipore] under UV. The reaction mixture was concentrated under vacuum. Flash chromatography of the residue [silica gel, CH_3OH:CH_2Cl_2 = 5:95 (v/v)] yielded compound **9** as a pale yellow oil (52.0 mg, 55.5%). IR (KBr, cm^{-1}) 3173, 3018, 2924, 2187, 2122, 2086, 1674, 1652, 1590, 1560, 1502, 1418, 1344, 1292, 1284, 1240, 1142, 1103, 1079, 942, 874, 824. ^{1}H NMR (600 MHz, CD_3OD): δ 9.1 (dd, *J* = 4.2, 1.8 Hz, 1H), 9.03 (dd, *J* = 4.8, 1.8 Hz, 1H), 8.89 (dd, *J* = 7.8, 4.2 Hz, 1H), 8.38 (dd, *J* = 7.8, 4.2 Hz, 1H), 8.11 (s 1H), 7.82 (q, *J* = 4.2 Hz, 1H), 7.73 (q, *J* = 4.2 Hz, 1H), 3.79 (t, *J* = 6 Hz, 2H), 3.40 (t, *J* = 6.6 Hz, 2H). ^{13}C NMR (150 MHz, CD_3OD) δ151.16, 151.10, 146.91, 146.14, 137.35, 135.20, 133.55, 132.34, 130.36, 129.92, 125.13, 124.79, 45.48, 35.21. HRMS (ESI) calcd. for $C_{15}H_{13}N_3S_2$ $[M+H]^+$: 298.0473, found 298.0459.

2.5. MS analysis procedures of synthesized compounds

The samples were diluted in methanol to approximately 1 M concentration. A sample solution (1 µL) was introduced by flow injection analysis (FIA) without a chromatographic column except for compound **7** where 2 µL was injected. The solvent system was 1:1 methanol:water with 0.1% formic acid. Ions were delivered to the mass spectrometer with an electrospray ionization (ESI) source. The nebulizer pressure was 50 PSIG. at 325 °C and nitrogen drying gas flow was 12 mL/min. The capillary voltage was 3000 V for all samples. For compound **6** (Boc protected), the fragmentor voltage was 150 V. Data were collected in the m/z range of 100-3200. Spectra were collected at a rate

of 2 spectra/s allowing for 4903 transients/spectrum. For compound **7**, the fragmentor voltage was 70 V. Data were collected in the m/z range of 500-2000. Spectra were acquired at a rate of 1 spectra/s allowing for 9978 transients/spectrum.

2.6. Preparation of G-quadruplex DNA and duplex DNA for CD and UV experiments

The G-quadruplex DNA strand (**G1**, 100 μM) was dissolved in a mixture (100 μL) of lithium cacodylate buffer (10 mM, pH 7.0) and KCl (50 mM) and incubated at 90 °C for 10 min, slowly cooled to 25°C, and incubated at 4 °C overnight. Similarly, duplex **D1** (complementary strands of S1 and S2, 100 μM each) was dissolved in a mixture of lithium cacodylate buffer (10 mM, pH 7.0) and KCl (150 mM) and incubated at 90 °C for 10 min, slowly cooled to 25°C, and incubated at 4 °C overnight. All solutions were stored at 4 °C for further use.

2.7. Preparation of G-quadruplex DNA for ESI mass spectrometry experiments

G1 (100 μM) in 150 mM NH_4OAc solution was heated to 95 °C for 5 min followed by cooling slowly to room temperature and incubated at 4°C overnight.

2.8. Thermal denaturation analysis monitored by CD

The mixture solutions (200 μL) of **G1** (5 μM) in lithium cacodylate buffer (10 mM, pH 7.0) and KCl (50 mM) in the absence or presence of a ligand (Phen, neomycin, and **7**, 10 μM) were prepared. The CD spectra were recorded at 290 nm as a function of increasing temperature (25-85 ˚C) at a heating rate of 0.5 ˚C/min. Melting profiles were converted into a folded faction based on a published procedure (40), and the melting temperatures were determined at the 0.5 folded fraction.

2.9. CD titration

Aliquots of a stock solution containing compound **7** were gradually added into a solution (2.0 mL) of **G1** (5 μM) in lithium cacodylate (10 mM, pH 7.0) and 50 mM KCl at 20 °C. The final molar ratios of **7** to **G1** were varied from 0 to 5. After each addition, the solution was gently mixed and incubated for 5 min for equilibrium before collecting the spectrum. The overall volume change during the titration was kept less than 1% of the initial volume. CD spectra were recorded as a function of wavelength (200-400 mm, 100 nm/min scan speed, 0.5 nm data pitch) using a 1 cm pathlength quartz cuvette. Each spectrum was averaged over three scans.

2.10. Thermal denaturation analysis monitored by UV

The mixture solutions (1 mL) of **D1** (1 μM) in lithium cacodylate buffer (10 mM, pH 7.0) and KCl (150 mM) in the absence or presence of a ligand (Phen, neomycin, and **7**, 10 μM) were prepared. The UV melting curves were recorded at 260 nm as a function of temperature (20-85 °C, heating rate: 0.5 °C/min). Melting profiles were converted into a folded faction, and the melting temperatures were determined at the 0.5 folded fraction.

2.11. *Fluorescent intercalator displacement assay*

A reaction solution containing 0.25 μM DNA (G-quadruplex (**G1**) or duplex (**D1**) in lithium cacodylate (10 mM, pH 7.0) and KCl (50 mM) was incubated with 0.5 μM thiazole orange (TO) for 30 min in the dark. Aliquots of a ligand were added to this mixture solution and equilibrated for 5 min in the dark before measurement. The fluorescence spectra (Ex: 501 nm, slit width: 5.0 nm, scan speed 120 nm/min) were recorded from 510-650 nm after each addition. The percent fluorescence displacement (%F) was calculated at λ_{max} by using the formula %FI. displacement=100-[(FA/FA$_0$)×100], where FA$_0$ is the initial fluorescence intensity in the absence of a ligand, and FA is the fluorescence intensity upon addition of a ligand.

2.12. Isothermal Titration Calorimetry (ITC)

In a typical experiment, 2 μL aliquots of compound **7** (200 μM) were injected from a 264 μL rotating syringe (125 rpm) into an isothermal sample cell containing 185 μL of a telomeric G-quadruplex (**G1**) (20 μM/strand) or a duplex DNA (**D1**) solution (10 μM/strand) at 25 °C. The corresponding control experiment was carried out by injecting 2 μL aliquots of compound **7** (200 μM) into a solution of buffer alone. The duration of each injection was 4 s, and the delay between injections was 120 s. The initial delay prior to the first injection was 100 s. A heat burst curve (microcalories per second vs. seconds) was generated from each injection. The area under each curve was calculated using the NanoAnalyzer software (Version 3.8.0) to yield a measure of the heat associated with that injection. The heat of ligand binding to DNA associated with that injection was obtained by subtracting the heat associated with each ligand-buffer injection from the corresponding heat associated with each ligand-DNA injection.

2.12. Preparation of cell lysate for TRAP assay

Approximately 1 x 10^7 HeLa cells were suspended in CHAPS buffer (1 mL) and incubated on ice for 30 min. The supernatant was collected after spinning the sample at 12,000 x g for 10 min and stored at -80℃.

2.13. TRAP assay

The 5′-[^{32}P] end-labeled TS primer (0.1 μg) was incubated in a reaction mixture (50 μL) [buffer: Tris-HCl (20 mM, pH 8.3), $MgCl_2$ (1.5 mM), KCl (63 mM), 0.05% Tween 20, EGTA (1 mM)] with cell lysate (1 μL), RP (0.1 μg, reverse primer for telomerase extended products), NT (0.1 μg, primer for polymerase as internal standard), TSNT (0.01 amol, template for NT primer), 2 units of Taq polymerase, dNTP mix (50 μM), and ligand (3.125-100 μM) at 30℃ for 30 min and 94℃ for 2 min to deactivate telomerase. The reaction mixture was then incubated using a 3-step PCR method (94 ℃ for 20 s, 59 ℃ for 30 s, and 72 ℃ for 30 s) with a total of 25 cycles. The residues were concentrated and resuspended in formamide loading buffer (7 μL). Analytical separation was carried out using 10% denaturing polyacrylamide gel [5% crosslink, 45% urea w/w].

2.14. Docking procedure

The geometry optimization of compound **7** was carried out at the hybrid density functional B3LYP level (41) with 6-31G(d) (42, 43) basis set using Gaussian'09 (44) program package. The Natural bond order (NBO) analysis (45, 46) was carried out to calculate the atomic charges on the optimized geometries. **G1** structure for docking simulation was modeled after the solution structure of complex of platinum(II) based ligand with human telomeric G-quadruplex (PDB id: 5Z80) (47) whose structure was obtained from RCSB protein data bank (48). In the complex structure, the bound ligand molecule was removed. The resulting template has two more A residues at the 5'-end and one additional A at the 3'-end in comparison to **G1**. In the NMR structure, Adenine-25 was mutated to thymine, and residues Adedine-1, 2, and 26 were truncated to yield the structure of **G1** for docking studies. The flexible ligand docking experiments were carried out using the DOCK 6.9 program (49, 50). Analyses of docked structures and docked image creations were carried out using UCSF Chimera program (51).

*2.14. ESI-MS analysis of complex formation between **G1** and 7*

G1 (20 μM) and compound **7** at various concentrations (0, 20, 40, 60, and 80 μM) were mixed as 50% methanol-water solutions. The mixed solutions were injected into a Thermo Fisher Orbitrap

Fusion Tribrid Mass Spectrometer at a rate of 5 μL/min. The ion spray voltage was set to -2,250 V and ion transfer tube temperature to 300 °C. Nitrogen sheath and auxiliary gas flows were 45 and 0 arbitrary units, respectively. MS spectra were recorded in the *m/z* range from 1400 to 1800 with an average of 150 scans. Data were collected and analyzed using the Xcalibur 4.0 software.

3. Results and Discussion

3.1. Synthesis of phenanthroline-neomycin conjugate 7

As shown in Scheme 1, neomycin precursor **5** was synthesized based on published procedures (52). The C5" position of the ring III of neomycin (Scheme 1) was used for conjugation. The modification of this site has a minimal effect on the structure of neomycin and its binding affinity to several nucleic acid structures as previously reported (52, 53). All six amino groups of neomycin (**1**) were protected using di-tert-butyl dicarbonate to yield compound **2**. Conversion of the 5" primary hydroxyl group of **2** into 2,4,6-triisopropylbenzenesulfonylate followed by reaction with sodium azide yielded compound **4**. The synthesis of compound **9** was accomplished by reacting phenanthroline amine **8** (54) with TCDP in DMF. Coupling of **9** with **5** yielded Boc-protected phenanthroline-neomycin conjugate **6**. Removal of Boc groups of **6** in the presence of trifluoroacetic acid yielded the desired compound **7**.

Insert Scheme 1

3.2. Fluorescence Intercalator Displacement (FID) assay

The binding of a telomeric G-quadruplex (**G1**) or a duplex (**D1**) with **7**, phenanthroline (Phen), and neomycin was first assessed using the Fluorescence Intercalator Displacement (FID) Assay (55). In this assay, thiazole orange (TO) was first bound to G-quadruplex DNA (**G1**), and the pre-bound TO was successively displaced out of DNA by the addition of a ligand of interest. The amount of ligand needed to displace 50% of pre-bound TO is defined as $^{G4}DC_{50}$ for G-quadruplex and $^{ds}DC_{50}$ for duplex DNA. Low DC values represent the high binding affinity of the ligand towards DNA. Neomycin is known to coordinate with metal ions (56). An initial study of the binding of **7** to **G1** in the presence of Ni^{2+} did not show enhanced binding compared with that of **7** alone (Figure S1 of the supporting information). Therefore, it is possible that Ni^{2+} could not effectively coordinate with the Phen moiety of **7** due to the interference of neomycin at the concentration range used. Hence, in this report, we are presenting data with Ni^{2+}-free conditions in the following studies. As shown in Figure

1, the corresponding rank order of the $^{G4}DC_{50}$ values was **7** < Phen-Ni < neomycin << Phen. The $^{G4}DC_{50}$ value for **7** (0.9 μM) was impressively low, 50-fold less than that of neomycin (49.8 μM) and more than 500-fold less than that of phenanthroline alone (> 500 μM). The low $^{G4}DC_{50}$ values for **7** suggested a strong displacement of TO from **G1** by **7**. It is noteworthy that these values are much lower than those obtained for other 5-substituted phenanthroline derivatives (**10** and **11**, Scheme 1) that contain amino-side chains. The $^{G4}DC_{50}$ values for **10** and **11** are 83.2 μM and 72.3 μM, respectively, as previously reported (11). The significant difference in $^{G4}DC_{50}$ values amongst **7**, **10**, and **11** suggested that the structured amino-containing binding motif (neomycin) can significantly enhance the binding with G-quadruplex DNA. Using the same conditions, the $^{ds}DC^{50}$ values for these compounds were also measured with a DNA duplex (**D1**). The $^{ds}DC^{50}$ values for **7** and neomycin are 3.4 μM and 5.7 μM, respectively. The relative selectivity of G-quadruplex over duplex DNA was determined by the ratio of $^{ds}DC_{50}/^{G4}DC_{50}$. The rank order for such selectivity was **7** (3.8) > neomycin (0.11). It is clear that compound **7** binds more preferentially to G4 than duplex DNA. Interestingly, neomycin has a smaller $^{ds}DC^{50}$ value (5.7 μM) than its $^{G4}DC_{50}$ value (49.8 μM). Phen binds to both duplex and G-quadruplex DNA very weakly based on the FID data. Both of the $^{G4}DC_{50}$ and $^{ds}DC^{50}$ values for Phen are over 500 μM; therefore, its selectivity of G4 over duplex DNA is negligible. An FID experiment of a mixture of neomycin and Phen (1:1 molar ratio) was also carried out. The $^{G4}DC_{50}$ value for the mixture is 9.0 μM, much smaller than those of neomycin (49.8 μM) and Phen (> 500 μM), indicating that the simultaneous binding of neomycin and Phen to G-quadruplex DNA has a minor synergistic effect. As a comparison, this value is 10-fold greater than that of **7** (0.9 μM). Hence, conjugation of neomycin with Phen via covalent bonds provides a more significant enhancement of binding with G-quadruplex DNA than merely mixing two ligands. It is noteworthy that **7** shows more remarkably enhanced binding with G-quadruplex DNA when compared to duplex DNA. The $^{ds}DC^{50}$ value (4.5 μM) of the mixture of neomycin and Phen is similar to the values of neomycin (5.7 μM) and **7** (3.4 μM). The binding of duplex DNA by **7** could mainly result from the non-specific binding by electrostatic interactions of cationic charges of the neomycin moiety.

Insert Figure 1

3.3. Interactions of 7 with DNA monitored by CD and UV

The ability of **7** to stabilize **G1** was confirmed using thermal denaturation of **G1** monitored by circular dichroism. As shown in Figure 2A, the representative folded fractions of **G1** in the absence and presence of a ligand (10 μM) are plotted as a function of temperature. The melting temperature (T_m) of **G1** was measured to be 61.0 ± 0.6 °C. In the presence of neomycin or Phen at 10 μM, the T_m values were 60.6 ± 0.3 and 60.8 ± 0.5 °C, respectively. Both neomycin and Phen could not stabilize **G1** under this condition. Phen did not increase the T_m value of **G1**, which is consistent with previous studies (11). In the presence of **7** at 10 μM, the T_m value was 66.6 ± 0.3 °C, a 5.6 °C increment as compared with that of **G1**. When incubating **G1** with neomycin (10 μM) and Phen (10 μM), no increment of T_m (61.0 ± 0.8 °C) was observed. Therefore, the stabilization effect of **7** toward **G1** must result from a synergistic enhancement of binding affinity by conjugating neomycin and phenanthroline together. Similar results were obtained from thermal denaturation monitored by UV at 295 nm (Figure S2 of the supporting information).

Evidence of the interaction between **7** and **G1** also came from monitoring the CD spectral changes when titrating a solution of **G1** with **7** at various concentrations. As shown in Figure 2B, the native folding of **G1** in K^+ adopts a hybrid-type topology with a maximum (+) around 292 nm, a shoulder (+) centered around 270 nm, a weak band (+) with a maximum around 250 nm, and a band (-) with a maximum around 235 nm, which is consistent with previous reports (57, 58). Titration of **G1** with **7** did not lead to an overall topological change of **G1**. Up to a ligand to DNA molar ratio of 3, a gradual increase in the intensity of the band (-) at 235 nm, the band (+) at 250 nm, and the band (+) around 292 nm was observed, respectively, suggesting that a further stabilization of the folded conformation (59) induced by interactions of **7** with **G1**. When the ligand to DNA molar ratio was above 3, a slight decrease in the intensities of these three bands occurred. In addition, the band (+) at 292 showed a redshift up to 300 nm during the course of titration. It is known that the lateral or diagonal loops of G-quadruplexes greatly affect the shape of their CD spectra (57). As indicated by the docking studies in the following section, the phenanthroline moiety of compound **7** could form π-π stacking interaction with an adenine in the loop (Figure 5B). At high ligand to DNA molar ratios, it is plausible that the neomycin moiety of several molecules of **7** could interact with the loops of **G1** via non-specific interactions, causing further redshift in band maxima.

The stabilization effect of neomycin, **7**, and Phen on a duplex DNA (**D1**) was investigated using thermal denaturation monitored by UV (Figure S3 of the supporting information). None of them showed a noticeable stabilization effect on the melting of **D1**, suggesting a weak binding of compound **7** with duplex DNA.

Insert Figure 2

3.4. Binding stoichiometry determined by ESI mass spectrometry

Mixtures of **7** and **G1** at a molar ratio ranging from 1:1 to 1:4 were analyzed using electrospray ionization (ESI) mass spectrometry, and a solution of **G1** was used as control. A mass spectrum representing a mixture of **G1** and **7** ([**G1**]:[**7**] = 1:2) is shown in Figure 3. The formation of the G-quadruplex structure was confirmed by the peak at *m/z* 1459.85, representing the ion $[\mathbf{G1}+2NH_4^+-7H^+]^{5-}$. The inclusion of two NH_4^+ ions is a distinct indication of the presence of three G-quartets in the G-quadruplex (60). Compound **7** was found to form a 1:1 complex with **G1**, indicated by the ion $[\mathbf{G1}+2NH_4^+ + \mathbf{7} - 7H^+]^{5-}$ at *m/z* 1642.13. The relative abundance of the complex is higher than those of free intact G-quadruplex when the molar ratio of **7** to **G1** is larger than 1, suggesting the strong tenancy of **7** to bind with G-quadruplex. It is noteworthy that varying the molar ratios of **7** and **G1** did not lead to different binding stoichiometries (Figure S4 of the supporting information).

Insert Figure 3

3.5. Thermodynamic parameters determined by Isothermal Titration Calorimetry (ITC)

The thermodynamics of a ligand (**7** or neomycin) binding to a telomeric G-quadruplex (**G1**) and a 26-mer duplex (**D1**) were determined using isothermal titration calorimetry (ITC) (61, 62). Figure 4 shows the representative ITC profiles (upper panels) resulting from a series of injections of **7** (200 μM) into a solution (20 μM) of **G1** (A) and **D1** (B) in K^+ at 25 °C. Calorimetric datum from injections of **7** into K^+ phosphate buffer under the same experimental conditions is used as blank for the heat of dilution (Figure S5 of the supporting information). The dotted lines (Figure 4, lower panels) show the resulting corrected injection heats (by subtracting the blank data for corrections of dilution effects) plotted as a function of the [**7**]/[DNA] molar ratio. Both binding isotherms can be fitted with different binding models provided in the TA Instrument's NanoAnalyze software (version 3.8.0). At 25 °C, the binding isotherm of **7** with **G1** (Figure 4A, lower panel) reveals a complex binding process, indicative of two binding events. The data best fit a multiple-sites model with a 90%

confidence level and result in two association constants (K_as), $(8.9\pm2.4)\times10^8$ M^{-1} and $(3.5\pm0.5)\times10^5$ M^{-1}. Based on the K_a values, the first binding event is a tight binding with a sharp transition, and the second binding event shows a gradual slope towards the binding saturation of **G1** by **7**, suggesting a relatively weak binding. Binding enthalpies for the two events were determined to be ΔH_1 [-(37.3±1.6) kJ/mol] and ΔH_2 [-(32.3±0.5) kJ/mol], indicative of highly enthalpically favored binding for both events. The first binding event is entropy favorable with a $T\Delta S$ value of +13.8 kJ/mol. According to a survey of thermodynamic signatures for ligand-DNA binding mode (63), groove binding is predominantly entropically driven, while intercalation is enthalpically driven. Our observation suggests that the tight-binding event could involve both groove-binding and π-π stacking, implying a synergetic binding effect between Phen and neomycin. The second binding event is slightly entropy unfavorable with a $T\Delta S$ value of -0.7 kJ/mol. The presence of the first binding event was highlighted by a separate ITC titration experiment in which a series of injections of **7** (200 μM) was titrated into a solution (40 μM) of **G1** to reach a final mole ratio of approximately 3 (Figure S6 of the supporting information).

The overall stoichiometry for binding of **7** to **G1** in the K^+ solution was determined to be approximately five ligands per G-quadruplex DNA. The sizeable binding stoichiometry suggests the second (weak) binding event may be associated with non-specific binding. It is noted that only a 1:1 binding stoichiometry was obtained from the ESI/MS experiments, as mentioned above. This discrepancy could result from the stability variations of ligand-DNA complexes in the solution phase and the gas phase of experimental conditions; therefore, the binding of **7** to weaker binding sites (non-specific binding) might not be observed in the ESI/MS experiments. At 25 °C, the binding isotherm of **7** with **D1** (Figure 4B, lower panel) best fits an independent (single-site) model with a 90% confidence level and result in an association constant of $(5.9\pm0.3)\times10^4$ M^{-1}. It is evident that the binding of **7** with **D1** is much weaker than both binding events of **7** with **G1** when comparing K_a values. The results obtained here are consistent with the aforementioned biophysical studies, in which compound **7** binds preferentially to telomeric G4 over duplex DNA. The binding of neomycin with **G1** at 25 °C shows a much lower association constant of $(6.1\pm0.2)\times10^3$ M^{-1} (Figure S7 of the supporting information). Given that Phen does not bind to G4s and weak binding of neomycin with **G1**, the strong binding of **7** with **G1** must come from covalently tethering neomycin and Phen.

Insert Figure 4

3.6. Molecular docking

Plausible binding modes of **7** with human telomeric G-quadruplex DNA was investigated using the DOCK 6.9 program. Because the G4 structure of the exact sequence used this work is not available in the data bank, we modeled **G1** structure using the NMR solution structure (PDB id: 5Z80) of the complex formed by a platinum ligand and a human telomeric G-quadruplex as the initial point. It is noted that the G-quadruplex-forming regions [$AGGGTT(AGGG)_3$] of **G1** and 5Z80 are identical. Upon manual removal of the platinum ligand and modification of a few residues at the 5' and 3'-positions, the resulting G4 structure has the same sequence as **G1** and is a hybrid-type topology. The simple docking results show that compound **7** can bind in the original binding site of the hybrid G-quadruplex, where the platinum ligand was found in the solution NMR structure. The most energetically favorable binding mode (Figure 5A) of **7** has the phenanthroline ring stack on top of the base pair in the G-quadruplex through π-π stacking and the neomycin moiety in the groove of the G-quadruplex. Further analysis shows π-π stacking between the phenanthroline ring of **7** and residues of adenine-7 and guanine-8 (Figure 5B) and hydrogen bonding interactions of the neomycin moiety with guanine-21 and the phosphate backbone of residues 19-21 (Figure 5C). The proposed binding mode is cohesive with the synergistic effect observed from biophysical studies. Using docking simulation, we also found several binding modes that do not interfere with each other. A representative binding mode of **G1** with three molecules of **7** is presented in Figure S9 of the supporting information. In addition, non-specific interactions between **G1** and **7** are plausible due to the electrostatic interactions of the neomycin moiety with DNA backbones.

Insert Figure 5

3.7. Inhibition of human telomerase activity by compound 7

Upon confirming the interactions between **7** and the telomeric G4, inhibition of human telomerase activity *in vitro* was investigated using a modified TRAP assay. As shown in Figure 6, a known telomerase inhibitor BIBR (64) (50 μM) was used as a control. The extension product bands in the lane for BIBR were negligible compared to those in the positive control lane (no ligand) while the PCR product band was clearly observed, suggesting that BIBR inhibited telomerase but not polymerase in the reaction. In contrast to BIBR, TMPyP4, a potent G4 ligand (65, 66), fully inhibited

the activities of telomerase and polymerase. No telomerase extension and PCR product bands (IS band disappeared) could be observed. The large stacking surface of TMPyP4 could intercalate into duplex DNA at this high concentration (50 μM) and thus block polymerase activity. These results were consistent with previously reported data (11, 12). As shown in Figure 6, compound **7** selectively inhibits the telomerase activity while it has no effect on the polymerase activity in the concentration range of 1.6 to 12.5 μM. The inhibition of telomerase activity by **7** could be unambiguously observed at 3.1 μM. Such inhibition is clearly concentration-dependent. At 12.5 μM, the activity of telomerase is greatly inhibited while the polymerase activity remains unaffected (IS band observed). It is noteworthy that the observed inhibition concentration (3.1 μM) is much lower than those of other 5-substituted phenanthrolines such as **10** and **11**, both of which did not show any noticeable inhibition effect even at concentrations as high as 50 μM (11). Furthermore, the potent inhibition of telomerase activity by compound **7** should not result from the effect of the neomycin moiety because neomycin does not show any inhibition effect even at a concentration of 100 μM (data not shown).

Insert Figure 6

4. Conclusion

In summary, the data here demonstrate that structured amino-containing side chains such as neomycin can be used as a suitable binding motif for 5-substituted phenanthroline based G4 ligands and telomerase inhibitors. The observed enhancement is significant, considering that Phen alone cannot effectively bind to G4s due to its relatively small stacking surface compared with the surface area of a G-quartet. Following the same concept, such side chains could also be used to conjugate with other G4 stacking ligands. Further investigations of the binding of **7** with other biologically relevant G4s such as c-Myc G-quadruplex DNA will be carried out in due course. This approach may open a new direction for designing novel telomerase inhibitors.

Acknowledgments

We are grateful for financial support from the University of the Pacific and support for purchasing an isothermal titration calorimeter from the National Science Foundation (MRI-1828179). We also thank Professor William K. Chan's lab (University of the Pacific) for the HeLa cell lysate.

Note

The authors declare no conflict of interest.

Data availability statement

The authors confirm that the data supporting the findings of this study are available within the article and its supplementary materials.

Supplementary data

NMR spectra of compounds **6**, **7** and **9**, FID titration profiles, mass spectra of **G1** and **7** mixtures, ITC profiles, and UV thermal denaturation profiles are presented.

References

1. Burge S, Parkinson GN, Hazel P, Todd AK, Neidle S (2006) Quadruplex DNA: sequence, topology and structure. *Nucleic Acids Res;***34**: 5402-15.
2. Davis JT (2004) G-quartets 40 years later: from 5'-GMP to molecular biology and supramolecular chemistry. *Angew Chem Int Ed Engl;***43**: 668-98.
3. Biffi G, Tannahill D, McCafferty J, Balasubramanian S (2013) Quantitative visualization of DNA G-quadruplex structures in human cells. *Nat Chem;***5**: 182-6.
4. Huppert JL, Balasubramanian S (2005) Prevalence of quadruplexes in the human genome. *Nucleic Acids Res;***33**: 2908-16.
5. Todd AK, Johnston M, Neidle S (2005) Highly prevalent putative quadruplex sequence motifs in human DNA. *Nucleic Acids Res;***33**: 2901-7.
6. Bedrat A, Lacroix L, Mergny JL (2016) Re-evaluation of G-quadruplex propensity with G4Hunter. *Nucleic Acids Res;***44**: 1746-59.
7. Chambers VS, Marsico G, Boutell JM, Di Antonio M, Smith GP, Balasubramanian S (2015) High-throughput sequencing of DNA G-quadruplex structures in the human genome. *Nat Biotechnol;***33**: 877-81.
8. Neidle S (2017) Quadruplex nucleic acids as targets for anticancer therapeutics. *Nat Rew Chem;***1**: 0041.
9. Rhodes D, Lipps HJ (2015) G-quadruplexes and their regulatory roles in biology. *Nucleic Acids Res;***43**: 8627-37.
10. Tian T, Chen Y-Q, Wang S-R, Zhou X (2018) G-Quadruplex: A Regulator of Gene Expression and Its Chemical Targeting. *Chem;***4**: 1314-44.

11. Liu W, Wang S, Dotsenko IA, Samoshin VV, Xue L (2017) Arylsulfanyl groups - suitable side chains for 5-substituted 1,10-phenanthroline and nickel complexes as G4 ligands and telomerase inhibitors. *J Inorg Biochem;***173**: 12-20.

12. Wang S, Yang D, Singh M, Joo H, Rangel VM, Tran A, et al. (2019) Thiazole orange - Spermine conjugate: A potent human telomerase inhibitor comparable to BRACO-19. *Eur J Med Chem;***175**: 20-33.

13. De Cian A, Lacroix L, Douarre C, Temime-Smaali N, Trentesaux C, Riou JF, et al. (2008) Targeting telomeres and telomerase. *Biochimie;***90**: 131-55.

14. Balasubramanian S, Hurley LH, Neidle S (2011) Targeting G-quadruplexes in gene promoters: a novel anticancer strategy? *Nat Rev Drug Discov;***10**: 261-75.

15. Nishikawa T, Kuwano Y, Takahara Y, Nishida K, Rokutan K (2019) HnRNPA1 interacts with G-quadruplex in the TRA2B promoter and stimulates its transcription in human colon cancer cells. *Sci Rep;***9**: 10276.

16. Pagano B, Amato J, Iaccarino N, Cingolani C, Zizza P, Biroccio A, et al. (2015) Looking for efficient G-quadruplex ligands: evidence for selective stabilizing properties and telomere damage by drug-like molecules. *ChemMedChem;***10**: 640-9.

17. Luedtke NW (2009) Targeting G-Quadruplex DNA with Small Molecules. *Chimia;***63**: 134-9.

18. Monchaud D, Teulade-Fichou MP (2008) A hitchhiker's guide to G-quadruplex ligands. *Org Biomol Chem;***6**: 627-36.

19. Chitranshi P, Xue L (2011) Utilizing G-quadruplex formation to target 8-oxoguanine in telomeric sequences. *Bioorg Med Chem Lett;***21**: 6357-61.

20. De Cian A, Delemos E, Mergny JL, Teulade-Fichou MP, Monchaud D (2007) Highly efficient G-quadruplex recognition by bisquinolinium compounds. *J Am Chem Soc;***129**: 1856-7.

21. Burger AM, DAi F, Schultes CM, Beszka AP, Moore MJ, Double JA, et al. (2005) The G-quadruplex-interactive molecule BRACO-19 inhibits tumor growth, consistent with telomere targeting and interference with telomerase function. *Cancer Res;***65**: 1489-96.

22. Bhasikuttan AC, Mohanty J (2015) Targeting G-quadruplex structures with extrinsic fluorogenic dyes: promising fluorescence sensors. *Chem Commun (Camb);***51**: 7581-97.

23. Wu S, Wang L, Zhang N, Liu Y, Zheng W, Chang A, et al. (2016) A Bis(methylpiperazinylstyryl)phenanthroline as a Fluorescent Ligand for G-Quadruplexes. *Chemistry;***22**: 6037-47.

24. Beauvineau C, Guetta C, Teulade-Fichou MP, Mahuteau-Betzer F (2017) PhenDV, a turn-off fluorescent quadruplex DNA probe for improving the sensitivity of drug screening assays. *Org Biomol Chem;***15**: 7117-21.

25. Medeiros-Silva J, Guedin A, Salgado GF, Mergny JL, Queiroz JA, Cabrita EJ, et al. (2017) Phenanthroline-bis-oxazole ligands for binding and stabilization of G-quadruplexes. *Biochim Biophys Acta Gen Subj;***1861**: 1281-92.

26. Chung WJ, Heddi B, Hamon F, Teulade-Fichou MP, Phan AT (2014) Solution structure of a G-quadruplex bound to the bisquinolinium compound Phen-DC(3). *Angew Chem Int Ed Engl;***53**: 999-1002.

27. Amato J, Iaccarino N, Pagano B, Morigi R, Locatelli A, Leoni A, et al. (2014) Bis-indole derivatives with antitumor activity turn out to be specific ligands of human telomeric G-quadruplex. *Front Chem;***2**: 54.

28. Lavrado J, Ohnmacht SA, Correia I, Leitao C, Pisco S, Gunaratnam M, et al. (2015) Indolo[3,2-c]quinoline G-quadruplex stabilizers: a structural analysis of binding to the human telomeric G-quadruplex. *ChemMedChem;***10**: 836-49.

29. Funke A, Weisz K (2019) Thermodynamic signature of indoloquinolines interacting with G-quadruplexes: Impact of ligand side chain. *Biochimie;***157**: 142-8.

30. Kaul M, Barbieri CM, Kerrigan JE, Pilch DS (2003) Coupling of Drug Protonation to the Specific Binding of Aminoglycosides to the A Site of 16S rRNA: Elucidation of the Number of Drug Amino Groups Involved and their Identities. *J Mol Biol;***326**: 1373-87.

31. Kaul M, Pilch DS (2002) Thermodynamics of aminoglycoside-rRNA recognition: the binding of neomycin-class aminoglycosides to the A site of 16S rRNA. *Biochemistry;***41**: 7695-706.

32. Arya DP, Xue L, Willis B (2003) Aminoglycoside (neomycin) preference is for A-form nucleic acids, not just RNA: results from a competition dialysis study. *J Am Chem Soc;***125**: 10148-9.

33. Ranjan N, Andreasen KF, Kumar S, Hyde-Volpe D, Arya DP (2010) Aminoglycoside binding to Oxytricha nova telomeric DNA. *Biochemistry;***49**: 9891-903.

34. Kaiser M, De Cian A, Sainlos M, Renner C, Mergny JL, Teulade-Fichou MP (2006) Neomycin-capped aromatic platforms: quadruplex DNA recognition and telomerase inhibition. *Org Biomol Chem;***4**: 1049-57.

35. Xue L, Xi H, Kumar S, Gray D, Davis E, Hamilton P, et al. (2010) Probing the recognition surface of a DNA triplex: binding studies with intercalator-neomycin conjugates. *Biochemistry;***49**: 5540-52.

36. Xue L, Charles I, Arya DP (2002) Pyrene-neomycin conjugate: dual recognition of a DNA triple helix. *Chem Commun (Camb);*70-1.

37. Arya DP, Xue L, Tennant P (2003) Combining the best in triplex recognition: synthesis and nucleic acid binding of a BQQ-neomycin conjugate. *J Am Chem Soc;***125**: 8070-1.

38. Xue L, Ranjan N, Arya DP (2011) Synthesis and spectroscopic studies of the aminoglycoside (neomycin)--perylene conjugate binding to human telomeric DNA. *Biochemistry;***50**: 2838-49.

39. Ranjan N, Davis E, Xue L, Arya DP (2013) Dual recognition of the human telomeric G-quadruplex by a neomycin-anthraquinone conjugate. *Chem Commun (Camb);***49**: 5796-8.

40. Mergny JL, Lacroix L (2003) Analysis of thermal melting curves. *Oligonucleotides;***13**: 515-37.

41. Becke AD (1993) Density ‐ functional thermochemistry. III. The role of exact exchange. *J Chem Phys;***98**: 5648-52.

42. Krishnan R, Binkley JS, Seeger R, Pople JA (1980) Self ‐ consistent molecular orbital methods. XX. A basis set for correlated wave functions. *J Chem Phys;***72**: 650-4.

43. McLean AD, Chandler GS (1980) Contracted Gaussian basis sets for molecular calculations. I. Second row atoms, Z=11–18. *J Chem Phys;***72**: 5639-48.

44. Frisch MJ, Trucks GW, Schlegel HB, Scuseria GE, Robb MA, Cheeseman JR, et al. (2009) Gaussian 09. *Gaussian 09*. Wallingford, CT, USA: Gaussian, Inc.

45. Foster JP, Weinhold F (1980) Natural hybrid orbitals. *J Am Chem Soc;***102**: 7211-8.

46. Reed AE, Curtiss LA, Weinhold F (1988) Intermolecular interactions from a natural bond orbital, donor-acceptor viewpoint. *Chem Rev;***88**: 899-926.

47. Liu W, Zhong YF, Liu LY, Shen CT, Zeng W, Wang F, et al. (2018) Solution structures of multiple G-quadruplex complexes induced by a platinum(II)-based tripod reveal dynamic binding. *Nat Commun;***9**: 3496.

48. Protein Data Bank(PDB) [http://www.rcsb.org].

49. Lang PT, Brozell SR, Mukherjee S, Pettersen EF, Meng EC, Thomas V, et al. (2009) DOCK 6: Combining techniques to model RNA–small molecule complexes. *Rna;***15**: 1219-30.

50. Allen WJ, Balius TE, Mukherjee S, Brozell SR, Moustakas DT, Lang PT, et al. (2015) DOCK 6: Impact of new features and current docking performance. *J Comput Chem;***36**: 1132-56.

51. Pettersen EF, Goddard TD, Huang CC, Couch GS, Greenblatt DM, Meng EC, et al. (2004) UCSF Chimera--a visualization system for exploratory research and analysis. *J Comput Chem;***25**: 1605-12.

52. Luedtke NW, Liu Q, Tor Y (2003) RNA-ligand interactions: affinity and specificity of aminoglycoside dimers and acridine conjugates to the HIV-1 Rev response element. *Biochemistry;***42**: 11391-403.

53. Xue L, Ranjan N, Arya DP (2011) Synthesis and spectroscopic studies of the aminoglycoside (neomycin)--perylene conjugate binding to human telomeric DNA. *Biochemistry;***50**: 2838-49.

54. Dotsenko IA, Curtis M, Samoshina NM, Samoshin VV (2011) Convenient synthesis of 5-aryl(alkyl)sulfanyl-1,10-phenanthrolines from 5,6-epoxy-5,6-dihydro-1,10-phenanthroline, and their activity towards fungal β-d-glycosidases. *Tetrahedron;***67**: 7470-8.

55. Monchaud D, Allain C, Teulade-Fichou MP (2006) Development of a fluorescent intercalator displacement assay (G4-FID) for establishing quadruplex-DNA affinity and selectivity of putative ligands. *Bioorg Med Chem Lett;***16**: 4842-5.

56. Jeżowska-Bojczuk M, Szczepanik W, Mangani S, Gaggelli E, Gaggelli N, Valensin G (2005) Identification of Copper(II) Binding Sites in the Aminoglycosidic Antibiotic Neomycin B. *Eur J Inorg Chem;***2005**: 3063-71.

57. Del Villar-Guerra R, Trent JO, Chaires JB (2018) G-Quadruplex Secondary Structure Obtained from Circular Dichroism Spectroscopy. *Angew Chem Int Ed Engl;***57**: 7171-5.

58. Zhang Z, Dai J, Veliath E, Jones RA, Yang D (2010) Structure of a two-G-tetrad intramolecular G-quadruplex formed by a variant human telomeric sequence in K+ solution: insights into the interconversion of human telomeric G-quadruplex structures. *Nucleic Acids Res;***38**: 1009-21.

59. Bianco S, Musetti C, Waldeck A, Sparapani S, Seitz JD, Krapcho AP, et al. (2010) Bis-phenanthroline derivatives as suitable scaffolds for effective G-quadruplex recognition. *Dalton Trans;***39**: 5833-41.

60. Guo X, Liu S, Yu Z (2007) Bimolecular quadruplexes and their transitions to higher-order molecular structures detected by ESI-FTICR-MS. *J Am Soc Mass Spectrom;***18**: 1467-76.

61. Pagano B, Mattia CA, Giancola C (2009) Applications of isothermal titration calorimetry in biophysical studies of G-quadruplexes. *Int J Mol Sci;***10**: 2935-57.

62. Haq I, Trent JO, Chowdhry BZ, Jenkins TC (1999) Intercalative G-Tetraplex Stabilization of Telomeric DNA by a Cationic Porphyrin1. *J Am Chem Soc;***121**: 1768-79.

63. Chaires JB (2006) A thermodynamic signature for drug-DNA binding mode. *Arch Biochem Biophys;***453**: 26-31.

64. Pascolo E, Wenz C, Lingner J, Hauel N, Priepke H, Kauffmann I, et al. (2002) Mechanism of human telomerase inhibition by BIBR1532, a synthetic, non-nucleosidic drug candidate. *J Biol Chem;***277**: 15566-72.

65. Nagesh N, Buscaglia R, Dettler JM, Lewis EA (2010) Studies on the site and mode of TMPyP4 interactions with Bcl-2 promoter sequence G-Quadruplexes. *Biophys J;***98**: 2628-33.

66. Han FX, Wheelhouse RT, Hurley LH (1999) Interactions of TMPyP4 and TMPyP2 with quadruplex DNA. Structural basis for the differential effects on telomerase inhibition. *J Am Chem Soc;***121**: 3561-70.

Figure Legends

Scheme 1. Synthesis of phenanthroline derivatives (**7** and **9**). a) $(Boc)_2O$, DMF-H_2O, 60 °C, 78.0%; b) TPS-Cl, pyridine, r.t., 60.0%; c) NaN_3, DMF, 2h, 95.0%; d) H_2, Pd/C, Ethanol, overnight, quant.; e) **9**, pyridine, overnight, r.t., 45.0%; f) TFA, 30 min, 69.0%; g) TCDP, DMF, r.t., overnight, 56.0%.

Figure 1. The $^{ds}DC_{50}$ and $^{G4}DC_{50}$ values for compound **7**, neomycin (neo), Phen, a mixture of Phen and neomycin (1:1 molar ratio) from the FID assay. Buffer: 10 mM lithium cacodylate, 50 mM KCl, pH 7.0.

Figure 2. The CD melting profiles of **G1** in the absence and presence of neomycin and **7** (10 μM) in 50 mM KCl. [**G1**] = 5 μM. Buffer: 10 mM lithium cacodylate, pH 7.0.

Figure 3. A representative mass spectrum of a mixture solution of **G1** and **7** ([**G1**]:[**7**] = 1:2). The peak with the maximum intensity was set as the base peak (100%).

Figure 4. upper panel: ITC profiles of **G1** (20 μM) (A) and **D1** (10 μM) (B) titrated with **7** (200 μM) in a 10 mM potassium phosphate buffer with 133 mM KCl, pH 7.0 at 25 °C. lower panel: The dotted line represents the corrected injection heats plotted as a function of the [**7**]/[**G1**] (A) and [**7**]/[**D1**] (B) molar ratio. The smooth solid line reflects the calculated fit of the data using the binding models (multiple-sites for G4 and independent for duplex) from the software NanoAnalyze. Upward peaks represent an exothermic event.

Figure 5. A) Docked structure of compound **7** with a human telomeric G-quadruplex (**G1**). G-quadruplex is represented as surface colored by electrostatic potential, and the ligand is represented as ball and stick. B) π-π stacking interactions of the phenanthroline moiety with the top G-quartet of **G1**. C) Binding interactions of the neomycin moiety with the groove of **G1**. The distances are in Å.

Figure 6. TRAP reactions in the presence of **7** at concentrations of 12.5, 6.25, 3.13, and 1.56 μM (from left to right). Reactions in the presence of BIBR (50 μM) and TMPyP4 (50 μM) were carried out as comparisons. The reaction in the first left lane has no telomerase. IS: PCR product as internal standard (TSNT as template).

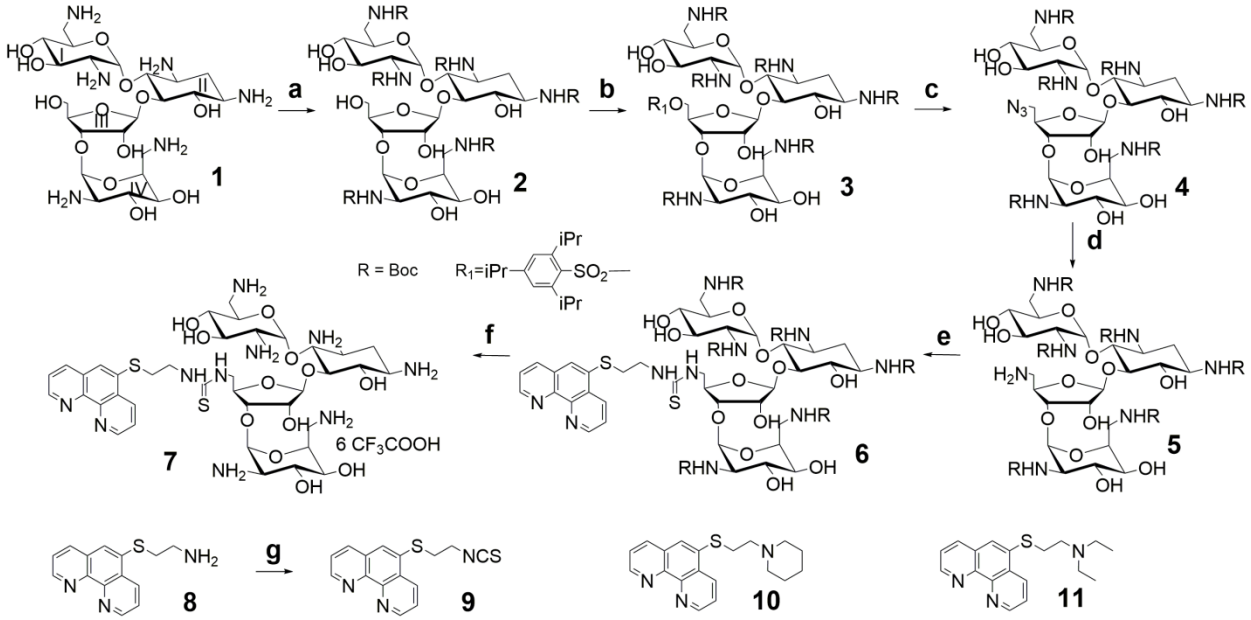

Scheme 1

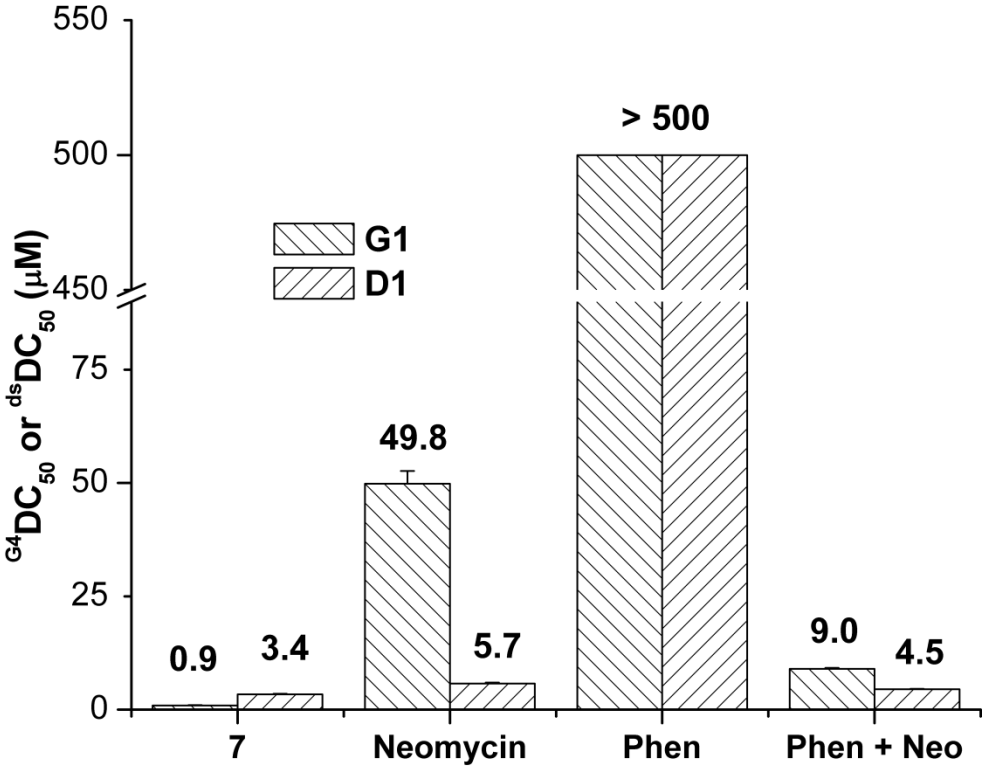

Figure 1

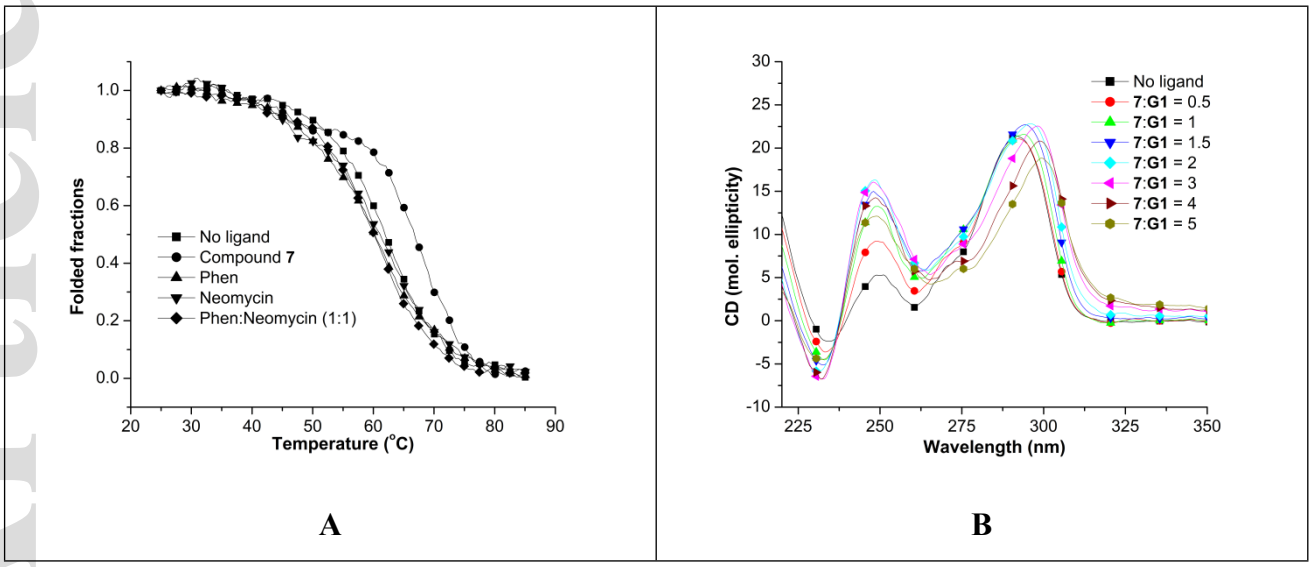

Figure 2

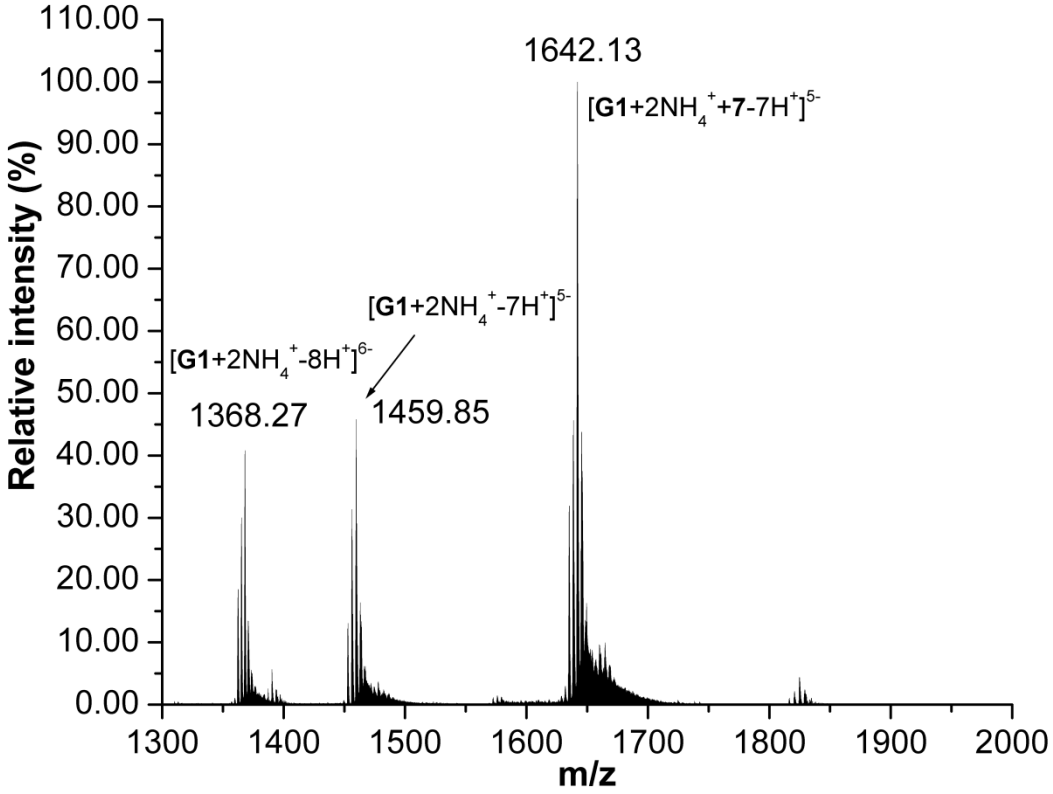

Figure 3

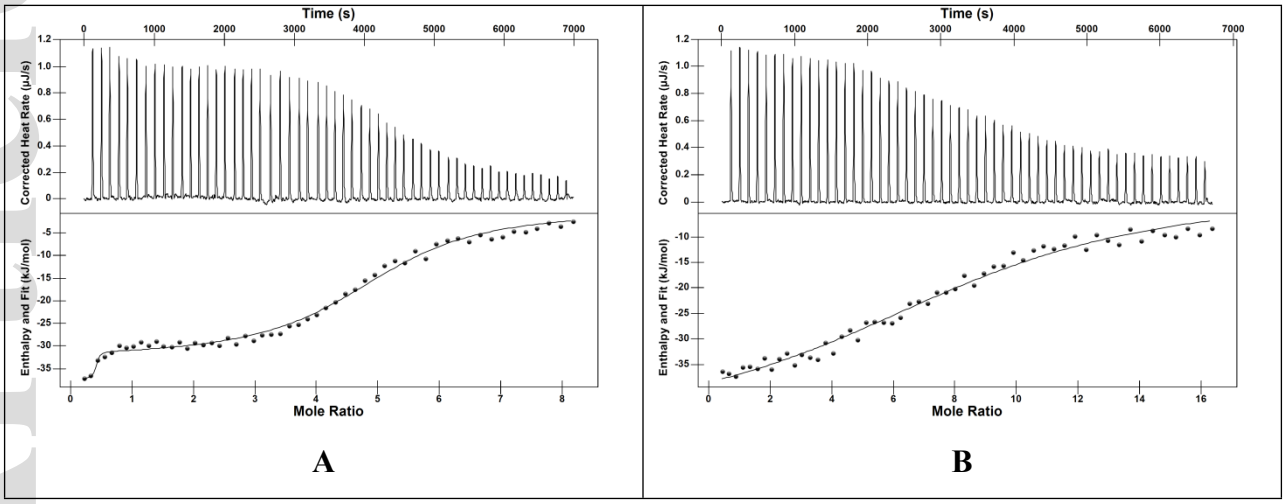

Figure 4

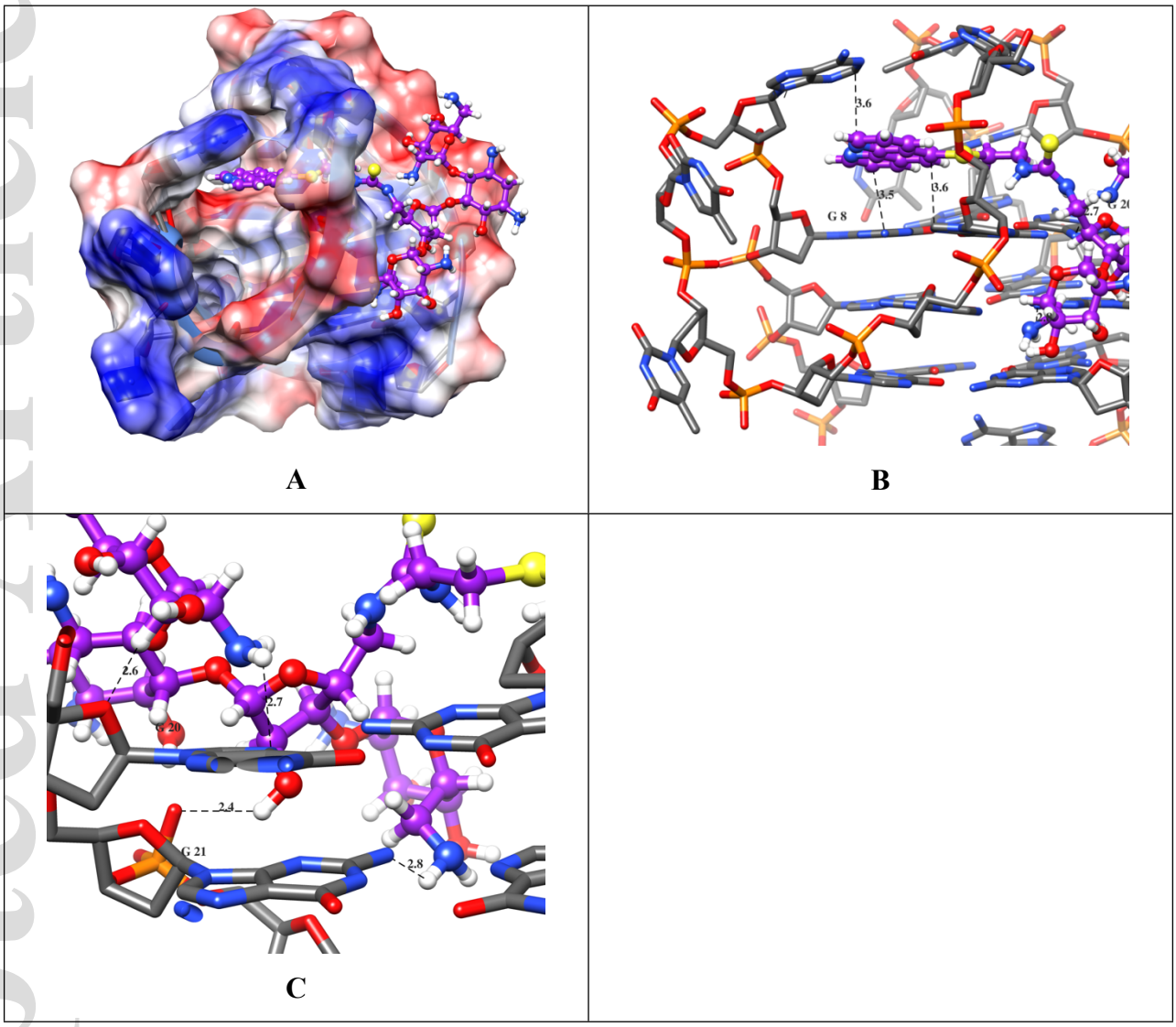

Figure 5

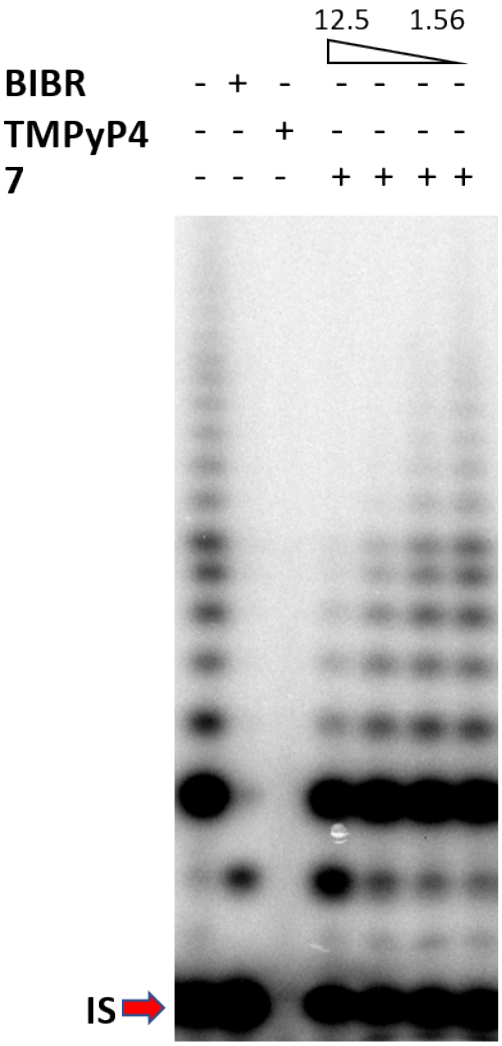

Figure 6